Supporting Information for

Deformation behavior and yield strength prediction of [112] oriented NbMoTaW refractory high entropy alloy nanowires

Taozhi Tian [a], Tao Fu [a, c, *], Mengye Duan [a], Hao Hu [a],
Chuanying Li [a], Xiang Chen [b, *], Xianghe Peng [a, *]

[a] *Department of Engineering Mechanics, Chongqing University, Chongqing 400044, China*
[b] *Institute for Advanced Sciences, Chongqing University of Posts and Telecommunications, Chongqing, 400065, China*
[c] *State Key Laboratory of Coal Mining Disaster Dynamics and Control, Chongqing University, Chongqing, 400044, China*

***Corresponding authors.**
Address: Department of Engineering Mechanics, Chongqing University, Chongqing 400044, China
E-mails: futao@cqu.edu.cn (T. F.); chenxiang@cqupt.edu.cn (X. C.); xhpeng@cqu.edu.cn (X. P.)

S1. Surface proportion

The radius of the nanowires is R, and the thickness of its surface layer is set to $0.866a$ (a is the lattice constant), so the cross-section area of the nanowire is $S_{NW}=\pi R^2$, the cross-section area of the surface layer is $S_{sur}=\pi R^2-\pi(R-0.886a)^2$, which leads to the surface-to-volume ratio (surface proportion) of $\alpha=S_{sur}/S_{NW}=1-(1-0.886a/R)^2$. Figure S1 shows the variation of surface proportion with R, which are consistent with those obtained directly by DXA in OVITO. It is important to note that, for comparative purposes, discrete points are employed to represent the surface proportions of the nanowires with different R. However, in the theoretical model presented in the main text, the radius R in the surface proportion can vary continuously, resulting in a smoother curve.

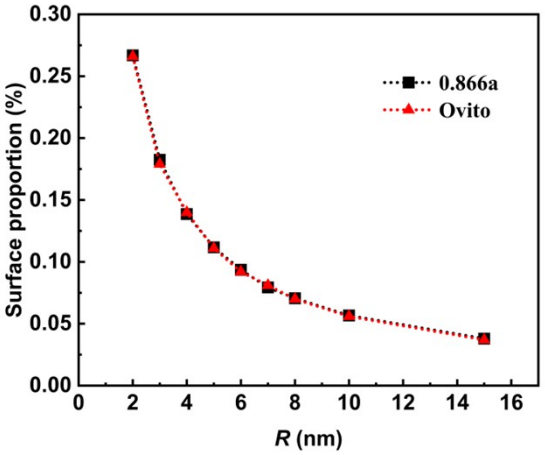

Fig. S1. Comparison of surface proportion calculated with different methods: black dots represent calculated

surface proportion using $\alpha=S_{sur}/S_{NW}=1-(1-0.886a/R)^2$, and the red dots represent the surface proportion identified by DXA in OVITO.

S2. Stacking fault energy

In this work, the dominant slip system of the nanowire is identified as {110} <111>. To calculate the generalized stacking fault energy (GSFE) of this slip system, a block sample is built, with its *x*, *y*, and *z* directions aligned as [1-11], [21-1], and [011], respectively. The sample is divided into upper and lower parts, enabling them to slide relative to each other in the *x*-direction by a distance of 1/2<111>*a* (*a* is the lattice constant). The energy variation during this slide is monitored and recorded. The GSFE is calculated using $\gamma_{SFE}=(E_1-E_0)/A$, where E_0 and E_1 are the energy before and after slide, respectively, and A represents the area of the sliding plane. The obtained forward and reverse GSFE curves of the NbMoTaW are shown in Fig. S2. Comparison of the two GSFE curves shows insignificant difference. Therefore, the average peak values of the two curves (1.363 J/m^2) is taken as the GSFE, which is close to that in the original documentation of the potential [1].

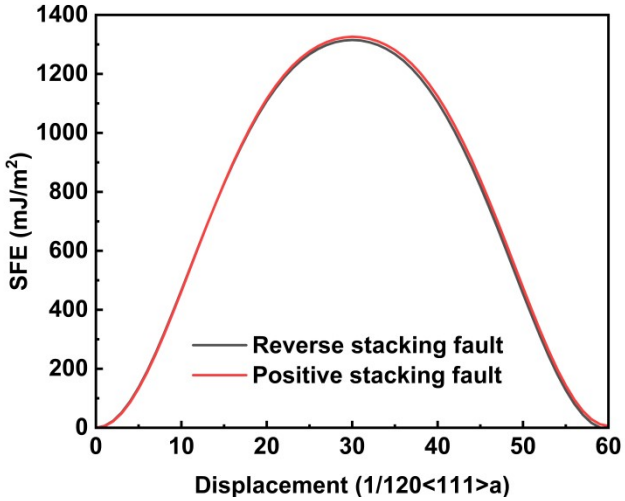

Fig. S2. GSFE curves of NbMoTaW along (011)[1-11], with red and black representing forward and reverse stacking fault energy curves, respectively.

S3. Surface energy

The surface energy is calculated using the NbMoTaW nanowires with different radii (R), using $\gamma_{SUR}=(E_{NW}-nE_{bulk})/A$, where E_{NW} is the total energy of the nanowire, E_{bulk} is the average energy per atom in the bulk sample without a surface, n is the total number of atoms in the nanowire, and A is the lateral area of the nanowire. Close to the predicted range, we select nanowires with 2 nm ≤ R ≤ 8 nm to calculate the surface energy. The results indicate that within this range, the surface energy does not exhibit significant fluctuations with changes in R [Fig. S3]. Therefore, the value of γ_{SUR} is determined using the average value obtained from the calculations across different R, specifically 2.615 J/m^2.

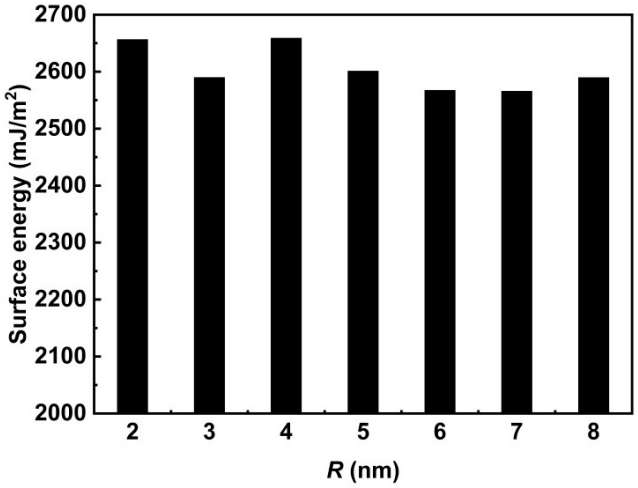

Fig. S3. Variation of surface energy of nanowires with radius.

S4. Model validation information

For metals that follow the HP relationship or small variation in the yield stress with sample size, such as Nb, V, and Ta, the nanowire sizes we used for our calculations may not be small enough to include the turning radius of these metals. The GSFEs and surface energies of the three metals are calculated and substituted into Eq. (7). Noticing that our theoretical formula is used to predict the yield stress in the IHP stage, and the IHP stages of these three metals are unknown, only the calculated minimum radius results (i.e., the yield stress value at R = 2 nm) and the theoretical formula are used for verification. As shown in Fig. S4, considering that the metal may still in the HP stage, our prediction results of R = 2 nm are slightly higher than the calculated results, but it still shows the good prediction ability of the theoretical formula.

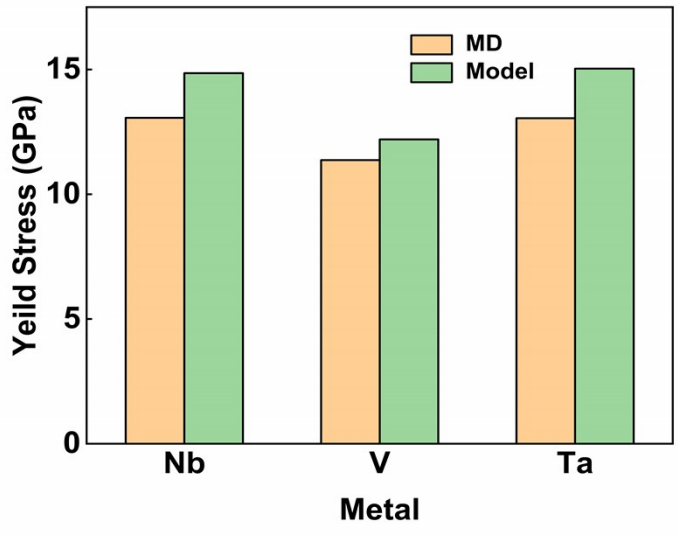

Fig. S4. Comparison of yield stresses of nanowires with R = 2 nm predicted using Eq. (7) with that obtained using MD simulations.

To evaluate the prediction capabilities of the model for other BCC metal nanowires, seven

groups of metal nanowires are built and tested, including the constituents in RHEAs and other BCC metals. The potential used for the tension simulations and the calculations of physical properties of these metals include: W [2], Mo [3], Fe [4], Nb [5], V [6], Ta [7] and WTa [8]. The calculated values of GSFE and surface energy are listed in Table S1.

Table S1. GSFEs and surface energies of different metals. The first column is calculated GSFEs, and the second and third columns are from literatures.

Metal	GSFE (J/m^2)			Surface energy (J/m^2)
W	1.655	1.633 [9]	1.786 [10]	3.518
Mo	1.025	0.92 [11]	1.46 [12]	3.013
Fe	0.783	0.98 [10]	0.949 [13]	2.254
Nb	0.708	0.674 [10]	0.678 [14]	2.24
V	0.596	0.58 [12]	0.701 [15]	1.646
Ta	0.763	0.66 [8]	0.84 [16]	2.295
WTa	1.243			2.708

S5. Size effect on yield stress of nanowires with different orientations

The variation of yield stress with radius in nanowires of different orientations is depicted in the Fig. S5. Among the three selected orientations, nanowires with [110] and [111] orientations exhibit a transition from HP to IHP relations as the yield stress varies with radius. In contrast, the nanowires with [001] orientation consistently maintain an HP relation. The calculated yield stresses for the three orientations show significant differences, with the yield stress for the [111] orientation being nearly twice that of the [001] orientation, indicating that the properties of BCC structured metals can vary significantly with changes in loading orientation.

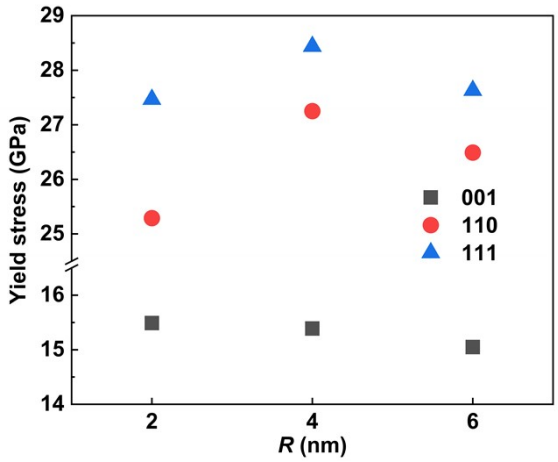

Fig. S5. Variations of yield stresses of nanowires with different orientations against nanowire radius.

References

1 X. G. Li, C. Chen, H. Zheng, Y. X. Zuo, and S. Y. P. Ong, Complex strengthening mechanisms in the NbMoTaW multi-principal element alloy. *Npj Computational Materials*. 6, 70 (**2020**)

2 P. Hiremath, S. Melin, E. Bitzek, and P. A. T. Olsson, Effects of interatomic potential on fracture behaviour in single- and bicrystalline tungsten. *Computational Materials Science*. 207, 111283 (**2022**)

3 J.-S. Kim, D. Seol, J. Ji, H.-S. Jang, Y. Kim, and B.-J. Lee, Second nearest-neighbor modified embedded-atom method interatomic potentials for the Pt-M (M = Al, Co, Cu, Mo, Ni, Ti, V) binary systems. *Calphad*. 59, 131-141 (**2017**)

4 M. I. Mendelev, S. Han, D. J. Srolovitz, G. J. Ackland, D. Y. Sun, and M. Asta, Development of new interatomic potentials appropriate for crystalline and liquid iron. *Philosophical Magazine*. 83, 3977-3994 (**2003**)

5 M. R. Fellinger, H. Park, and J. W. Wilkins, Force-matched embedded-atom method potential for niobium. *Physical Review B*. 81, 144119 (**2010**)

6 P. A. T. Olsson, Semi-empirical atomistic study of point defect properties in BCC transition metals. *Computational Materials Science*. 47, 135-145 (**2009**)

7 R. Ravelo, T. C. Germann, O. Guerrero, Q. An, and B. L. Holian, Shock-induced plasticity in tantalum single crystals: Interatomic potentials and large-scale molecular-dynamics simulations. *Physical Review B*. 88, 134101 (**2013**)

8 Y. C. Chen, J. Z. Fang, L. X. Liu, W. Y. Hu, N. Gao, F. Gao, and H. Q. Deng, Development of the interatomic potentials for W-Ta system. *Computational Materials Science*. 163, 91-99 (**2019**)

9 J. Qian, C. Y. Wu, J. L. Fan, and H. R. Gong, Effect of alloying elements on stacking fault energy and ductility of tungsten. *Journal of Alloys and Compounds*. 737, 372-376 (**2018**)

10 X. C. Zhang, S. Cao, L. J. Zhang, R. Yang, and Q. M. Hu, Unstable stacking fault energy and peierls stress for evaluating slip system competition in body-centered cubic metals. *Journal of Materials Research and Technology-Jmr&T*. 22, 3413-3422 (**2023**)

11 G. J. Ackland, and R. Thetford, An improvedN-body semi-empirical model for body-centred cubic transition metals. *Philosophical Magazine A*. 56, 15-30 (**1987**)

12 Y. Chen, X. Liao, N. Gao, W. Hu, F. Gao, and H. Deng, Interatomic potentials of W–V and W–Mo binary systems for point defects studies. *Journal of Nuclear Materials*. 531, 152020 (**2020**)

13 J. Zhao, Y. C. Jiang, L. Sun, H. R. Gong, and X. Gong, Effect of alloying elements on stacking fault energy and ductility of iron. *Vacuum*. 194, 110633 (**2021**)

14 J. Huang, H. Xing, and J. Sun, Structural stability and generalized stacking fault energies in β Ti–Nb alloys: Relation to dislocation properties. *Scripta Materialia*. 66, 682-685 (**2012**)

15 S. Z. Xu, Y. Q. Su, L. T. W. Smith, and I. J. Beyerlein, Frank-Read source operation in six body-centered cubic refractory metals. *Journal of the Mechanics and Physics of Solids*. 141, 104017 (**2020**)

16 Y. Mishin, and A. Y. Lozovoi, Angular-dependent interatomic potential for tantalum. *Acta Materialia*. 54, 5013-5026 (**2006**)